

Equivariant quantum circuits for learning on weighted graphs

Andrea Skolik,^{1,2} Michele Cattelan,² Sheir Yarkoni,^{1,2} Thomas Bäck,¹ and Vedran Dunjko¹

¹*Leiden University, Niels Bohrweg 1, 2333 CA Leiden, The Netherlands*

²*Volkswagen Data:Lab, Ungererstraße 69, 80805 Munich, Germany*

(Dated: May 13, 2022)

Variational quantum algorithms are the leading candidate for near-term advantage on noisy quantum hardware. When training a parametrized quantum circuit to solve a specific task, the choice of ansatz is one of the most important factors that determines the trainability and performance of the algorithm. Problem-tailored ansatzes have become the standard for tasks in optimization or quantum chemistry, and yield more efficient algorithms with better performance than unstructured approaches. In quantum machine learning (QML), however, the literature on ansatzes that are motivated by the training data structure is scarce. Considering that it is widely known that unstructured ansatzes can become untrainable with increasing system size and circuit depth, it is of key importance to also study problem-tailored circuit architectures in a QML context. In this work, we introduce an ansatz for learning tasks on weighted graphs that respects an important graph symmetry, namely equivariance under node permutations. We evaluate the performance of this ansatz on a complex learning task on weighted graphs, where a ML model is used to implement a heuristic for a combinatorial optimization problem. We analytically study the expressivity of our ansatz at depth one, and numerically compare the performance of our model on instances with up to 20 qubits to ansatzes where the equivariance property is gradually broken. We show that our ansatz outperforms all others even in the small-instance regime. Our results strengthen the notion that symmetry-preserving ansatzes are a key to success in QML and should be an active area of research in order to enable near-term advantages in this field.

I. INTRODUCTION

Combinatorial optimization problems are ubiquitous, be it in transportation and logistics, electronics, or scheduling tasks. These types of problems have also been studied in computer science and mathematics for decades. Many interesting combinatorial optimization problems that are relevant in industry today are NP-hard, so that no general efficient solution is expected to exist. For this reason, heuristics have gained much popularity, as they often provide high-quality solutions to real-world instances of many NP-hard problems. However, good heuristics require domain expertise in their design and they have to be defined on a per-problem basis. To circumvent hand-crafting heuristic algorithms, machine learning approaches for solving combinatorial optimization problems have been studied. One line of research in this area investigates using neural networks (NNs) to learn algorithms for solving combinatorial optimization problems [1, 2], which is known as *neural combinatorial optimization* (NCO). Here, NNs learn to solve combinatorial optimization problems based on data, and can then be used to find approximate solutions to arbitrary instances of the same problem. First approaches in this direction used supervised learning to find approximate solutions based on NN techniques from natural language processing [3]. A downside of the supervised approach is that it requires access to a large amount of training data in form of solved instances of the given problem, which requires solving many NP-hard instances of the problem to completion. At large problem sizes, this is a serious impediment for the practicability of this method. For this reason, reinforcement learning (RL) was introduced as a technique to train these heuristics. In RL, an agent does not learn based on a given data set, but by

interacting with an environment and gathering information in a trial-and-error fashion. These RL-based approaches have been shown to successfully solve even instances of significant size in problems with a geometric structure like the convex hull problem [4], chip placement [5] or the vehicle routing problem [6].

In most combinatorial optimization problems the instances are presented in a structured form, for instance as a graph, so the structure of the ML models underlying the above techniques can be chosen in an informed manner. In recent years the field that focuses on the study of exploiting this known structure, called geometric deep learning, has garnered a lot of interest [7]. This field studies the properties of common NN architectures, like convolutional NNs or graph NNs, through the lens of group theory and geometry and provides an understanding of why these structured types of models are the main drivers of recent advances in deep learning. The success of these models can largely be attributed to the fact that they preserve certain symmetries that are present in the training data, e.g., translation invariance in images in the case of convolutional NNs, or permutation invariance or equivariance in the case of graph NNs, as depicted in fig. 1.

When it comes to quantum computing, much work has been dedicated to understanding the structure for variational quantum algorithms [8] that address problems in optimization [9, 10] or chemistry [11, 12]. For quantum machine learning however, it is largely unknown which type of ansatz should be used for a given type of data. In absence of an informed choice, general architectures as the hardware efficient ansatz (HWEA) [13] are often used [14]. It is known that unstructured ansatzes like the HWEA scale badly as the width and depth of the circuit grows, most prominently because of the barren plateau phenomenon [15–

[17] where the gradients of a parametrized quantum circuit (PQC) vanish exponentially as the system size grows and thus render training impossible. This situation can be compared to the early days of NNs, where fully connected feedforward NNs were the standard architecture. These types of NNs suffer from similar trainability issues as unstructured quantum circuits [18]. The true break-throughs in deep learning were in part possible because more efficient architectures have been developed, like the convolutional NN for image recognition or the recurrent NN for time series.

In this work, we introduce a permutation equivariant quantum circuit architecture for weighted graphs and demonstrate that it significantly outperforms unstructured ansatzes. To evaluate these ansatzes on a complex learning task that is relevant for solving industry-related problems once scaled up in instance size, we study their performance in the context of neural combinatorial optimization to find approximate solutions to the Traveling Salesperson Problem (TSP). Our contributions are as follows.

- We introduce an equivariant ansatz for learning on weighted graphs.
- We evaluate the performance of this ansatz on the task of solving TSP instances and show that it performs well on instances with up to 20 cities (20 qubits).
- We numerically compare our ansatz to three non-equivariant ansatzes, and show that the more the equivariance property of the ansatz is broken, the worse performance becomes and that a simple hardware-efficient ansatz completely fails on this learning task.
- We analytically study the expressivity of our model at depth one, and show under which conditions there exists a parameter setting for any given TSP instance of arbitrary size for our ansatz that produces the optimal tour with the RL scheme that is applied in this work.

Our work illustrates the merit of using symmetry-preserving ansatzes for QML on the example of graph-based learning, and underlines the notion that in order to successfully apply variational quantum algorithms for ML tasks in the future, the usage of unstructured ansatzes that are popular in current QML research is limited as problem sizes grow. This work motivates further study of “geometric quantum learning” in the vein of the classical field of geometric deep learning, to establish more effective ansatzes for QML, as these are a prerequisite to efficiently apply quantum models on any practically relevant learning task in the near-term. The full code that was used to generate the numerical results in this work can be found on GitHub [19].

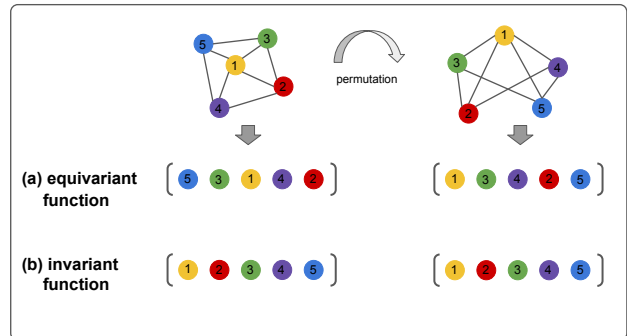


FIG. 1: Depiction of two functions that respect important symmetries of graphs: a) The permutation *equivariant* function will yield the same output values for each graph permutation, but reordered according to the reordering of nodes. The above example shows a simple function that outputs node features in the same order as they are fed into the function. b) An *invariant* function will yield the same output, regardless of the permutation. The above example shows a simple function that outputs node features in ascending order. Which of the two is preferable depends on the task at hand.

II. RELATED WORK

A. Geometric learning - quantum and classical

Learning approaches that utilize geometric properties of a given problem have lead to major successes in the field of ML, such as AlphaFold for the complex task of protein folding [20, 21] and have become an increasingly popular research field over the past few years. Arguably the prime example of a successful geometric model is the convolutional NN (CNN), which has been developed at the end of the 20th century in an effort to enable efficient training of image recognition models [22]. Since then, it has been shown that one of the main reasons that CNNs are so effective is that they are translation invariant: if an object in a given input image is shifted by some amount, the model will still “recognize” it as the same object and thus effectively requires fewer training data [7]. While CNNs are the standard architecture used for images, symmetry-preserving architectures have also been developed for time-series data in the form of recurrent NNs [23], and for graph data with GNNs [24]. GNNs have seen a surge of interest in the classical machine learning community in the past decade [24, 25]. They are designed to process data that is presented in graph form, like social networks [24], molecules [26], images [27] or instances of combinatorial optimization problems [1].

The first attempt to implement a geometric learning model in the quantum realm was made with the quantum convolutional NN in [28], where the authors introduce a translation invariant architecture motivated by classical convolutional NNs. Approaches to translate the GNN formalism to QNNs were taken in [29], where input graphs are represented in terms of a parametrized Hamiltonian, which is then used

to prepare the ansatz of a quantum model called a *quantum graph neural network* (QGNN). While the approach in [29] yields promising results, this work does not take symmetries of the input graph into account. The authors of [30] introduce the so-called *quantum evolution kernel*, where they devise a graph-based kernel for a quantum kernel method for graph classification. Again, their ansatz is based on alternating layers of Hamiltonians, where one Hamiltonian in each layer encodes the problem graph, while a second parametrized Hamiltonian is trained to solve a given problem. A proposal for a quantum graph convolutional NN was made in [31], and the authors of [32] propose directly encoding the adjacency matrix of a graph into a unitary to build a quantum circuit for graph convolutions. While all of the above works introduce forms of structured QML models, none of them study their properties explicitly from a geometric learning perspective or relate their performance to unstructured ansatzes.

The authors of [33] take the step to introduce an equivariant model family for graph data and generalize the QGNN picture to so-called *equivariant quantum graph circuits* (EQGCs). EQGCs are a very broad class of ansatzes that respect the connectivity of a given input graph. The authors of [33] also introduce a subclass of EQGCs called *equivariant quantum Hamiltonian graph circuits* (EH-QGCs), that includes the QGNNs by [29] as a special case. EH-QGCs are implemented in terms of a Hamiltonian that is constructed based on the input graph structure, and they are explicitly equivariant under permutation of vertices in the input graph. The framework that the authors of [33] propose can be seen as a generalization of the above proposals. Different from the above proposals, EQGCs use a post-measurement classical layer that performs the functionality of an aggregation function as those found in classical GNNs. In classical GNNs, the aggregation function in each layer is responsible for aggregating node and edge information in an equivariant or invariant manner. Popular aggregation functions are sums or products, as they trivially fulfill the equivariance property. In the case of EQGCs, there is no aggregation in the quantum circuit, and this step is offloaded to a classical layer that takes as input the measurements of the PQC. Additionally, the EQGC family is defined over unweighted graphs and only considers the adjacency matrix of the underlying input graph to determine the connectivity of the qubits. The authors of [33] also show that their EQGC outperforms a standard message passing neural network on a graph classification task, and thereby demonstrate a first separation of quantum and classical models on a graph-based learning task.

During preparation of our final manuscript, a work on invariant quantum machine learning models was released by the authors of [34]. They prove for a number of selected learning tasks whether an invariant quantum machine learning model for specific types of symmetries exists. Their work focuses on group invariance, and leaves proposals for NISQ-friendly equivariant quantum models as an open question.

Our proposal is most closely related to EH-QGCs, but with a number of deviations. First, our model is defined on weighted graphs and can therefore be used for learning tasks that contain node as well as edge features. Second, the initial state of our model is always the uniform superposition, which allows each layer in the ansatz to perform graph feature aggregation via sums and products of node and edge features, as we will discuss in section III. Third, we do not require a classical post-processing layer, so our EQC model is purely quantum. Additionally, in its simplest form as used in this work, the number of qubits in our model scales linearly with the number of nodes in the input graph, while the depth of each layer depends on the graph’s connectivity, and therefore it provides one answer to the question of a NISQ-friendly equivariant quantum model posed by [34].

B. Neural combinatorial optimization with reinforcement learning

The idea behind NCO is to use a ML model to learn a heuristic for a given optimization problem based on data. When combined with RL, this data manifests in form of states of an environment, while the objective is defined in terms of a reward function, as we will now explain in more detail. In the RL paradigm, the model, referred to as an *agent*, interacts with a so-called *environment*. The environment is defined in terms of its state space \mathcal{S} and action space \mathcal{A} , that can both either be discrete or continuous. The agent alters the state of the environment by performing an action $a \in \mathcal{A}$, whereafter it receives feedback from the environment in form of the following state $s' \in \mathcal{S}$, and a reward r that depends on the quality of the chosen action, given the initial state s . Actions are chosen based on a *policy* $\pi(a|s)$, which is a probability distribution of actions a given states s . The definition of the state and action spaces and the reward function depends on the given environment. In general, the goal of the agent is to learn a policy that maximizes the expected return G ,

$$G_t = \sum_{k=0}^{\infty} \gamma^k r_{t+k+1}, \quad (1)$$

where $\gamma \in [0, 1]$ is the *discount factor* that determines the importance of future rewards in the agent’s decision. The above definition of the expected return is for the so-called *infinite horizon*, where the interaction with the environment can theoretically go on to infinity. In practice, we usually work in environments with a *finite horizon*, where the above sum runs only over a predefined number of indices. There are many different approaches to maximize the expected return, and we refer the interested reader to [35] for an in-depth introduction.

In this work, we focus on so-called *Q-learning*, where the expected return is maximized in terms of *Q-values*. The values $Q(s, a)$ for each (s, a) pair also

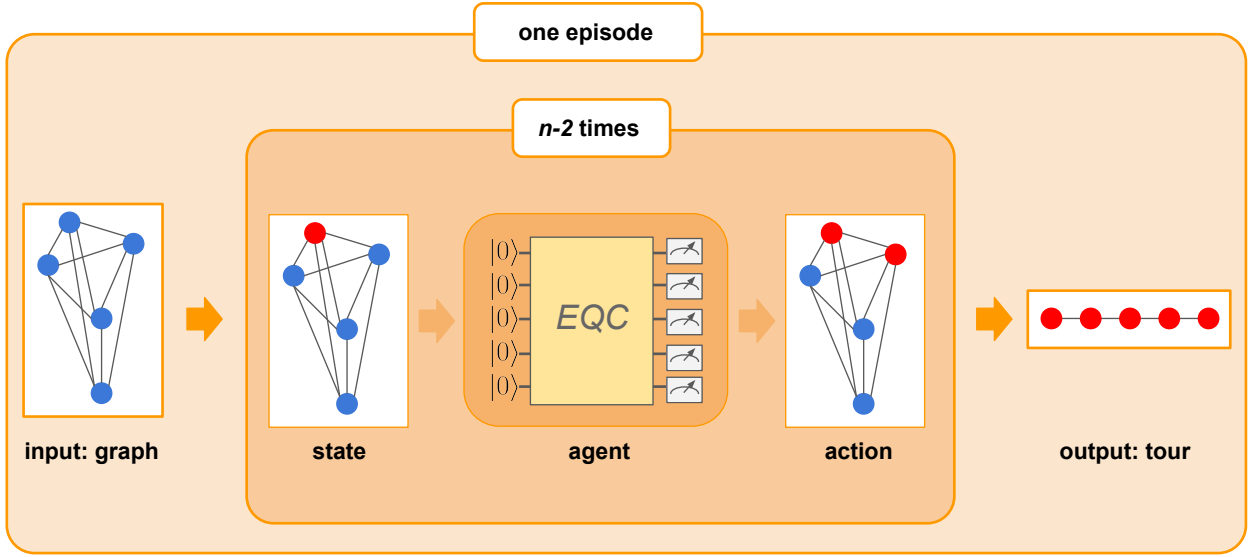


FIG. 2: An illustration of one episode in the TSP environment. The agent receives a graph instance as input, where the first node is already added to the proposed tour (marked red), which can always be done without loss of generality. In each time step, the agent proposes which node should be added to the tour next. After the second-to-last node has been selected, the agent returns a proposed tour.

represent the expected return following a policy π , but now conditioned on an initial state s_t and action a_t ,

$$Q(s, a) = \mathbb{E}_\pi[G_t | s = s_t, a = a_t]. \quad (2)$$

When the agent is implemented in form of a NN, the goal of the NN is to approximate the optimal Q-function Q^* . One popular method to use a NN as a function approximator for Q-learning is called the *deep Q-network* (DQN), and the resulting *DQN algorithm* [36]. In this algorithm, the NN is trained similarly as in the supervised case, but without a given set of labelled examples. Instead, the agent collects samples at training time by interacting with the environment. These samples are stored in a memory, out of which a batch of random samples is drawn for each parameter update step. Based on the agent's output, the label for a given (s, a) pair from the memory is computed as follows,

$$q = r_{t+1} + \gamma \cdot \max_a \hat{Q}_\theta(s_{t+1}, a), \quad (3)$$

and this label is then used to compute parameter updates. The update is not computed with the output of the function approximator Q , but by a copy \hat{Q} called the *target network*, which is updated with the current parameters of the function approximator at fixed intervals. The purpose of this target network is to stabilize training, and how often it is updated is a hyperparameter that depends on the environment. In

our case, the function approximator and target network are implemented as PQCs, while the parameter optimization is performed via the classical DQN algorithm. For more detail on implementing the DQN algorithm with a PQC as the function approximator, we refer the reader to [37–39].

1. Solving the Traveling Salesperson Problem with reinforcement learning

To evaluate the performance gains of an ansatz that respects certain symmetries relevant to the problem at hand, we apply our model to a practically motivated learning task on graphs. The TSP is a low-level abstraction of a problem commonly encountered in mobility and logistics: given a list of locations, find the shortest route that connects all of these locations without visiting any of them twice. Formally, given a graph $\mathcal{G}(\mathcal{V}, \mathcal{E})$ with vertices \mathcal{V} and weighted edges \mathcal{E} , the goal is to find a permutation of the vertices such that the resulting tour length is minimal, where a tour is a cycle that visits each vertex exactly once. A special case of the TSP is the 2D Euclidean TSP, where each node is defined in terms of its x and y coordinates in Euclidean space, and the edge weights are given by the Euclidean distance between these points. In this work, we deal with the symmetric Euclidean TSP on a complete graph, where the edges in the graph are undirected. This reduces the number of possible tours from $n!$ to $\frac{(n-1)!}{2}$. However, even in this reduced case the number of possible tours is already larger than 100k for instances with a modest number of ten cities,

and the TSP is a well-known NP-hard problem.

To solve this problem with a RL approach, we follow the strategy introduced in [4]. In this work, a classical GNN is used to solve a number of combinatorial optimization problems on graphs. The authors show that this approach can outperform dedicated approximation algorithms defined for the TSP, like the Christofides algorithm, on instances of up to 300 cities. One episode of this learning algorithm for the TSP can be seen in fig. 2, and a detailed description of the learning task as implemented in our work is given in section IV A.

III. EQUIVARIANT QUANTUM CIRCUIT

In this section, we formally introduce the structure of our equivariant quantum circuit (EQC) for learning tasks on weighted graphs that we use in this work. One well-known example of graph-based data are images, which are pixel values ordered on a 2D-grid with nearest-neighbor connections. Other types of data that are represented in graph form are, for example, social networks or molecules. In general, when learning based on graph data, there are two sets of features: node features and edge features. Depending on the specific learning task, it might be enough to use only one set of these features as input data, and the specific implementation of the circuit will change accordingly. As mentioned above, an example of an ansatz for cases where encoding node features suffices is the EQGC introduced in [33]. In our case, we use both node and edge features to solve TSP instances. In case of the nodes, we encode whether a node is already present in the partial tour at time step t to inform the node selection process described later in definition 2. For the edges, we simply encode the edge weights of the graph as these correspond to the distance between nodes in the 2D Euclidean graph. In this work, we use one qubit per node in the graph, but in general multiple qubits per node are also possible. We discuss the details of this in appendix A. We now proceed to define the ansatz in terms of encoding node information in form of α (see definition 1) and edge information in terms of the weighted graph edges $\varepsilon_{ij} \in \mathcal{E}$.

A. Ansatz structure and equivariance

Given a graph $\mathcal{G}(\mathcal{V}, \mathcal{E})$ with node features α and weighted edges \mathcal{E} , and trainable parameters $\beta, \gamma \in \mathbb{R}^p$, our ansatz at depth p is of the following form

$$|\mathcal{E}, \alpha, \beta, \gamma\rangle_p = U_N(\alpha, \beta_p) U_G(\mathcal{E}, \gamma_p) \dots U_N(\alpha, \beta_1) U_G(\mathcal{E}, \gamma_1) |s\rangle, \quad (4)$$

where $|s\rangle$ is the uniform superposition of bitstrings of length n ,

$$|s\rangle = \frac{1}{\sqrt{2^n}} \sum_{x \in \{0,1\}^n} |x\rangle, \quad (5)$$

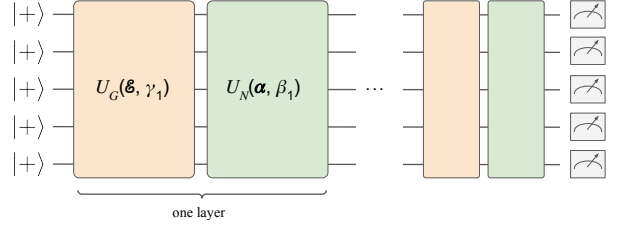


FIG. 3: EQC used in this work. Each layer consists of two parts: the first part U_G encodes edge features, while the second part U_N encodes node features. Each of the two parts is parametrized by one parameter β_l, γ_l , respectively.

$U_N(\alpha, \beta_j)$ with $R_x(\theta) = e^{-i\frac{\theta}{2}X}$, is defined as

$$U_N(\alpha, \beta_j) = \bigotimes_{l=1}^n R_x(\alpha_l \cdot \beta_j), \quad (6)$$

and $U_G(\mathcal{E}, \gamma_j)$ is

$$U_G(\mathcal{E}, \gamma_j) = \exp(-i\gamma_j H_G) \quad (7)$$

with $H_G = \sum_{(i,j) \in \mathcal{E}} \varepsilon_{ij} \sigma_z^{(i)} \sigma_z^{(j)}$ and \mathcal{E} are the edges of graph \mathcal{G} weighted by ε_{ij} . A 5-qubit example of this ansatz can be seen in fig. 3.

For $p = 1$, we have

$$\begin{aligned} |\mathcal{E}, \alpha, \beta, \gamma\rangle_1 &= U_N(\alpha, \beta) U_G(\mathcal{E}, \gamma) |s\rangle \\ &= \frac{1}{\sqrt{2^n}} \\ &\cdot \sum_{x \in \{0,1\}^n} \underbrace{\left(\cos \frac{\alpha_1 \beta}{2} + \dots - i \sin \frac{\alpha_l \beta}{2} - \dots - i \sin \frac{\alpha_n \beta}{2} \right)}_{\text{weighted bitflip terms}} \\ &\cdot \exp \left(\underbrace{\sum_{(i,j) \in \mathcal{E}} \text{diag}(Z_i Z_j)_{|x\rangle} \cdot -i \frac{\pi}{2} \gamma \varepsilon_{ij}}_{\text{edge weights}} \right) |x\rangle, \quad (8) \end{aligned}$$

where $\text{diag}(Z_i Z_j)_{|x\rangle} = \pm 1$ is the entry in the matrix corresponding to each $Z_i Z_j$ term, e.g., $I_1 \otimes \dots \otimes Z_i \otimes I_k \otimes \dots \otimes Z_j \otimes \dots \otimes I_n$, corresponding to the basis state $|x\rangle$. (E.g., the first term on the diagonal corresponds to the all-zero state, and so on.) We see that the first group of terms, denoted *weighted bitflip terms*, is a sum over products of terms that encode the node features. In other words, in the one-qubit case we get a sum over sine and cosine terms, in the two-qubit case we get a sum over products of pairs of sine and cosine terms, and so on. The terms in the second part of the equation denoted *edge weights* is the exponential of a sum over edge weight terms. As we start in the uniform superposition, each basis state's amplitude depends on all node and edge features, but with different signs and therefore different terms interfering constructively and destructively for every basis state. This can be regarded as a quantum version of the classical aggregation functions in GNNs as discussed

in section II. Similarly to the classical case where the k -th layer of a NN aggregates information over the k -local neighborhood of the graph, the terms in eq. (8) become more complex with each additional layer in the PQC.

The reader may already have observed that this ansatz is closely related to an ansatz that is well-known in quantum optimization: that of the quantum approximate optimization algorithm (QAOA) [9]. Indeed, our ansatz can be seen as a special case of the QAOA, where instead of using a cost Hamiltonian to encode the problem, we directly encode instances of graphs and apply the “mixer terms” in eq. (6) only to available nodes. This correspondence will later let us use known results for QAOA-type ansatzes at depth one [40] to derive exact analytical forms of the expectation values of our ansatz, and use these to study its expressivity.

As our focus is on implementing an ansatz that respects a symmetry that is useful in graph learning tasks, namely an equivariance under permutation of vertices of the input graph, we now show that each part of our ansatz respects this symmetry.

Theorem 1 (Permutation equivariance of the ansatz). *Let the ansatz be of the type as defined in eq. (4) with parameters $\beta, \gamma \in \mathbb{R}^p$ that represents an instance of a graph \mathcal{G} with weighted edges $\varepsilon_{ij} \in \mathcal{E}$. Let $P \in \mathbb{B}^{n \times n}$ be a permutation on the weighted adjacency matrix A of \mathcal{G} , and $\tilde{P} \in \mathbb{B}^{2^n \times 2^n}$ a matrix that maps the tensor product $|v_1\rangle \otimes |v_2\rangle \otimes \dots \otimes |v_n\rangle$ with $|v_i\rangle \in \mathbb{C}^2$ to $|v_{p(1)}\rangle \otimes |v_{p(2)}\rangle \otimes \dots \otimes |v_{p(n)}\rangle$. We call an ansatz that satisfies the following property equivariant under permutations of vertices in \mathcal{G} ,*

$$|\mathcal{E}, \alpha, \beta, \gamma\rangle_p = \tilde{P} |\mathcal{E}_{(P^T A P)}, \alpha, \beta, \gamma\rangle_p, \quad (9)$$

with $\mathcal{E}_{(P^T A P)}$ the graph edges after action of the permutation matrix on the adjacency matrix A of the given graph.

As mentioned before, our ansatz is closely related to the EH-QGCs in [33], and the authors of this work prove the equivariance of this type of circuit for unweighted adjacency matrices. In order to prove equivariance of our circuit, we have to generalize their result to the case where a weighted graph is encoded in form of a Hamiltonian and parametrized by a set of free parameters on these weights as described in eq. (4). In the non-parametrized case this is trivial, as edge weights are directly permuted as a consequence of the permutation of the adjacency matrix. When introducing parameters to the node and edge features however, we have to make sure that the parameters themselves preserve equivariance. As the parameters are not tied to the adjacency matrix but to the circuit itself, they need to be invariant under permutations of the input graph. To guarantee this, we choose to assign one node and edge parameter per layer, respectively, and this makes us arrive at the QAOA-type parametrization shown in eq. (4). For didactic reasons we provide a formal proof of our circuit’s equivariance in appendix A. Note that we formulate the theorem

in terms of the state vector $|\mathcal{E}, \alpha, \beta, \gamma\rangle_p$ instead of the unitary

$$U_N(\alpha, \beta_p) U_G(\mathcal{E}, \gamma_p) \dots U_N(\alpha, \beta_1) U_G(\mathcal{E}, \gamma_1),$$

as our initial state is always the uniform superposition. The equivariance of this unitary holds regardless of the initial state, however, when choosing an initial state that is different from the uniform superposition, the equivariance of the state vector only holds if that initial state is permutation invariant.

IV. QUANTUM NEURAL COMBINATORIAL OPTIMIZATION WITH THE EQC

In this section, we formally define the learning task that we address in this work, and the specific setup of the EQC and its observables. We show that each component of the QNCO scheme – Q-values and resulting tour – is equivariant under permutation of the vertices, and then analytically study the expressivity of our ansatz at depth one.

A. Formal definition of learning task and figures of merit

Our goal is to use the ansatz described in section III to train a model that, once trained, implements a heuristic to produce tours for the TSP. The TSP consists of finding a permutation of a set of cities such that the resulting length of a tour visiting each city in this sequence is minimal. The heuristic takes as input an instance of the TSP problem in form of a weighted 2D Euclidean graph $\mathcal{G}(\mathcal{V}, \mathcal{E})$ with $n = |\mathcal{V}|$ nodes representing the cities and edge weights $\varepsilon_{ij} = d(v_i, v_j)$, where $d(v_i, v_j)$ is the Euclidean distance between nodes v_i and v_j . Specifically, we are dealing with the symmetric TSP, where the edges in the graph are undirected. Given \mathcal{G} , the algorithm constructs a tour in $n - 2$ steps. Starting from a given (fixed) node in the proposed tour $T_{t=1}$, in each step t of the tour selection process the algorithm proposes the next node (city) in the tour. Once the second-before-last node has been added to the tour, the last one is also directly added, hence the tour selection process requires $n - 2$ steps. This can also be viewed as the process of successively marking nodes in a graph as they are added to a tour. In order to refer to versions of the input graph at different time steps where the nodes that are already present in the tour are marked, we now define the *annotated graph*.

Definition 1 (Annotated graph). *For a graph $\mathcal{G}(\mathcal{V}, \mathcal{E})$, we call $\mathcal{G}(\mathcal{V}, \mathcal{E}, \alpha^{(t)})$ the annotated graph at time step t . The vector $\alpha^{(t)} \in \{0, \pi\}^n$ specifies which nodes are already in the tour T_t ($\alpha_i^{(t)} = 0$) and which nodes are still available for selection ($\alpha_i^{(t)} = \pi$).*

In each time step of an episode in the algorithm, the model is given an annotated graph as input. Based on the annotated graph, the model should select the

next node to add to the partial tour T_t at step t . The annotation can be used to partition the nodes \mathcal{V} into the set of *available nodes* $\mathcal{V}_a = \{v_i | \alpha_i^{(t)} = \pi\}$ and the set of *unavailable nodes* $\mathcal{V}_u = \{v_i | \alpha_i^{(t)} = 0\}$. The node selection process can now be defined as follows.

Definition 2 (Node selection). *Given an annotated graph $\mathcal{G}(\mathcal{V}, \mathcal{E}, \boldsymbol{\alpha}^{(t)})$, the node selection process consist of selecting nodes in a tour in a step-wise fashion. To add a node to the partial tour T_t , the next node is selected from the set of available nodes \mathcal{V}_a . The unavailable nodes \mathcal{V}_u are ignored in this process.*

After $n-2$ steps, the model has produced a tour T_n . A depiction of this process can be found in fig. 2. To assess the quality of the generated tour, we compare the tour length $c(T_n)$ to the length of the optimal tour $c(T^*)$, where

$$c(T) = \sum_{\{i,j\} \in \mathcal{E}_T} \varepsilon_{ij} \quad (10)$$

is the sum of edge weights (distances) for all edges between the nodes in the tour, with $\mathcal{E}_T \subset \mathcal{E}$. We measure the quality of the generated tour in form of the approximation ratio

$$\frac{c(T_n)}{c(T^*)}. \quad (11)$$

The rewards in this environment are defined by the difference in overall length of the partial tour T_t at time step t , and upon addition of a given node v_l at time step $t+1$:

$$r(T_t, v_l) = -c(T_{t+1, v_l}) + c(T_t). \quad (12)$$

Note that we use the negative of the cost as a reward, as a Q-learning agent will always select the action that leads to the maximum expected reward.

The learning process is defined in terms of a DQN algorithm, where the Q-function approximator is implemented in form of a PQC (which is described in detail in section III). Here, we define the TSP in terms of an RL environment, where the set of states $\mathcal{S} = \{\mathcal{G}_i(\mathcal{V}, \mathcal{E}, \boldsymbol{\alpha}^{(t)}) \text{ for } i = 1, \dots, |\mathcal{X}| \text{ and } t = 1, \dots, n-1\}$ consists of all possible annotated graphs (i.e., all possible configurations of values of $\boldsymbol{\alpha}^{(t)}$) for each instance i in the training set \mathcal{X} . This means that the number of states in this environment is $|\mathcal{S}| = 2^{n-1}|\mathcal{X}|$. The action that the agent is required to perform is selecting the next node in each step of the node selection process described in definition 2, so the action space \mathcal{A} consists of a set of indices for all but the first node in each instance (as we always start from the first node in terms of the list of nodes we are presented with for each graph, so $\alpha_1^{(t)} = 0, \forall t$), and $|\mathcal{A}| = n-1$.

The Q-function approximator gets as input an annotated graph, and returns as output the index of the node that should next be added to the tour. Which index this is, is decided in terms of measuring an observable on each qubit corresponding to the available nodes \mathcal{V}_a . Depending on the last node added to the

partial tour, denoted as v_{t-1} , the observable for each available node v_l is defined as

$$O_{v_l} = \varepsilon_{v_{t-1}, v_l} Z_{v_{t-1}} Z_{v_l} \quad (13)$$

weighted by the edge weight $\varepsilon_{v_{t-1}, v_l}$, and the Q-value corresponding to each action is

$$Q(\mathcal{G}_i(\mathcal{V}, \mathcal{E}, \boldsymbol{\alpha}^{(t)}), v_l) = \langle \mathcal{E}, \boldsymbol{\alpha}^{(t)}, \boldsymbol{\beta}, \boldsymbol{\gamma} |_{\mathcal{P}} O_{v_l} | \mathcal{E}, \boldsymbol{\alpha}^{(t)}, \boldsymbol{\beta}, \boldsymbol{\gamma} \rangle_{\mathcal{P}}, \quad (14)$$

where the exact form of $|\mathcal{E}, \boldsymbol{\alpha}^{(t)}, \boldsymbol{\beta}, \boldsymbol{\gamma}\rangle_{\mathcal{P}}$ is described in section III. All unavailable nodes $v_l \in \mathcal{V}_u$ are not included in the node selection process, so we manually set their Q-values to a large negative number to exclude them, e.g.,

$$Q(\mathcal{G}_i(\mathcal{V}, \mathcal{E}, \boldsymbol{\alpha}^{(t)}), v_l) = -10000 \quad \forall v_l \in \mathcal{V}_u.$$

We also define a stopping criterion for our algorithm, which corresponds to the agent solving the TSP environment for a given instance size. As we aim at comparing the results of our algorithm to optimal solutions in this work, we have access to a labeled set of instances and define our stopping criterion based on these. However, note that the optimal solutions are not required for training, as a stopping criterion can also be defined in terms of number of episodes or other figures of merit that are not related to the optimal solution. In this work, the environment is considered as solved and training is stopped when the average approximation ratio of the past 100 iterations is < 1.05 , where an approximation ratio of 1 means that the agent returns the optimal solution for the instances it was presented with in the past 100 episodes. We do not set the stopping criterion at optimality for two reasons: i) it is unlikely that the algorithm finds a parameter setting that universally produces the optimal tour for all training instances, and ii) we want to avoid overfitting on the training data set. If the agent does not fulfill the stopping criterion, the algorithm will run until a predefined number of episodes is reached. In our numerical results shown in section V, however, most agents do not reach the stopping criterion of having an average approximation ratio below 1.05, and run for the predefined number of episodes instead. Our goal is to generate a model that is, once fully trained, capable of solving previously unseen instances of the TSP.

B. Equivariance of algorithm components

We showed in section III A that our ansatz of arbitrary depth is permutation equivariant. Now we proceed to show that the Q-values that are generated from measurements of this PQC, and the tour generation process as described in section IV A are equivariant as well. While the equivariance of all components of an algorithm is not a pre-requisite to harness the advantage gained by an equivariant model, knowing which parts of our learning strategy fulfill

this property provides additional insight for studying the performance of our model later. As we show that the whole node selection process is equivariant, we know that the algorithm will always generate the same tour for every possible permutation of the input graph for a fixed setting of parameters, given that the model underlying the tour generation process is equivariant. This is not necessarily true for a non-equivariant model, and simply by virtue of giving a permuted graph as input, the algorithm can potentially return a different tour.

Theorem 2 (Equivariance of Q-values). *Let $Q(\mathcal{G}_i(\mathcal{V}, \mathcal{E}, \alpha^{(t)}), v_l)$ as defined in eq. (14) be the Q-value corresponding to vertex v_l and graph \mathcal{G}_i annotated with the nodes contained in the partial tour T_t at step t of a given episode. Let p_n be a permutation of $n = |\mathcal{V}|$ elements, where the l -th element corresponds to the l -th vertex v_l and p_n^Q be a permutation that reorders the Q-values $Q(\mathcal{G}_i^{(t)}) = \{Q(\mathcal{G}_i^{(t)}, v_1), \dots, Q(\mathcal{G}_i^{(t)}, v_n)\}$ in correspondence to the reordering of the vertices by p_n . Then $Q(\mathcal{G}_i^{(t)}, v_l)$ is equivariant under permutation of the vertices v_l ,*

$$Q(\mathcal{G}_i^{(t)}, v_l) = Q(\mathcal{G}_i^{(t, p_n)}, v_{p_n^Q(l)}), \quad (15)$$

where $\mathcal{G}_i^{(t, p_n)}$ is the permuted graph at step t , and $v_{p_n^Q(l)}$ is the vertex corresponding to v_l after the permutation p_n .

Proof. We know from Theorem 1 that the ansatz that we use and therefore the expectation values $\langle O_{v_l} \rangle$ are permutation equivariant. The remaining terms in $Q(\mathcal{G}_i^{(t)}, v_l)$ (see eq. (14)) only depend on the edge weights of the graph \mathcal{G} . The edge weights are computed according to the graph's adjacency matrix, and are therefore re-ordered under a permutation of the vertices p_n and assigned to their corresponding permuted expectation values. By this, all terms in $Q(\mathcal{G}_i^{(t)}, v_l)$ are permutation equivariant. \square

As a second step to show that all components of our algorithm are permutation equivariant, it remains to show that the tours that our model produces as described in section IV A are also equivariant under permutations.

Theorem 3 (Equivariance of tours). *Let $T_t(\mathcal{G}_i, \beta, \gamma, v_0)$ be a tour generated by a permutation equivariant agent implemented with a PQC as defined in Theorem 1 and Q-values as defined in Theorem 2, for a fixed set of parameters β, γ and a given start node v_0 , where a tour is a cycle over all vertices $v_l \in \mathcal{V}$ that contains each vertex exactly once. Let p_n be a permutation of the vertices \mathcal{V} . The output tour is equivariant under permutation of the vertices,*

$$T_t(\mathcal{G}_i, \beta, \gamma, v_0) = T_t(\mathcal{G}_{i, p_n}, \beta, \gamma, v_{p_n(0)}). \quad (16)$$

Proof. We have shown in Theorem 2 that the Q-values of our model are permutation equivariant, meaning that a permutation of vertices results in a reordering

of Q-values to different indices. Action selection is done by $v_{t+1} = \operatorname{argmax}_v Q(\mathcal{G}_i^{(t)}, v)$, and the node at the index corresponding to the largest Q-value is chosen. To generate a tour, the agent starts at a given node v_0 and sequentially selects the following $n - 1$ vertices. Upon a permutation of the input graph, the tour now starts at another node index $v_{p_n(0)}$. Each step in the selection process can now be seen w.r.t. the original graph $\mathcal{G}_i^{(t)}$ and the permuted graph $\mathcal{G}_i^{(t, p_n)}$. As we have shown in Theorem 1, equivariance of the model holds for arbitrary input graphs, so in particular it holds for each $\mathcal{G}_i^{(t)}$ and $\mathcal{G}_i^{(t, p_n)}$ in the action selection process, and the output tour under the permuted graph is equal to the output tour under the original graph up to a renaming of the vertices. \square

C. Analysis of expressivity

In this section, we analyze under which conditions there exists a setting of β, γ for a given graph instance \mathcal{G}_i for our ansatz at depth one that can produce the optimal tour for this instance. Note that this does not show anything about constructing the optimal tour for a number of instances simultaneously with this set of parameters, or how easy it is to find any of these sets of parameters. Those questions are beyond the scope of this work. The capability to produce optimal tours at any depth for individual instances is of interest because first, we do not expect that the model can find a set of parameters that is close-to-optimal for a large number of instances if it is not expressive enough to contain a parameter setting that is optimal for individual instances. Second, the goal of a ML model is always to find similarities within the training data that can be used to generalize well on the given learning task, so the ability to find optimal solutions on individual instances is beneficial for the goal of generalizing on a larger set of instances. Additionally, how well the model generalizes also depends on the specific instances and the parameter optimization routine, and therefore it is hard to make formal statements about the general case where we find one universal set of parameters that produces the optimal solution for arbitrary sets of instances.

For our model at $p = 1$, we can compute the analytic form of the expectation values of our circuit as defined in eq. (13) and eq. (14) as the following, by a similar derivation as in [40],

$$\langle O_{v_l} \rangle = \varepsilon_{v_{t-1}, v_l} \cdot \sin(\beta\pi) \sin(\varepsilon_{v_{t-1}, v_l} \gamma) \cdot \prod_{\substack{(v_l, k) \in \mathcal{E} \\ k \neq v_{t-1}}} \cos(\varepsilon_{v_l, k} \gamma), \quad (17)$$

where v_{t-1} is the last node in the partial tour and v_l is the candidate node. In order to generate an arbitrary tour of our choice, in particular also the optimal tour, it suffices to guarantee that for a suitable choice of (fixed) γ , at each step in the node selection process the edge we want to add next to the partial tour has

highest expectation. One way we can do this is by controlling the signs of each sine and cosine term in eq. (17) such that only the expectation values corresponding to edges that we want to select are positive, and all others are negative.

To understand whether this is possible, we can leverage known results about the expressivity of the sine function. First, it is known that the function class $f(x) = \text{sign}(\sin(x\omega))$ parametrized by a single real-valued parameter ω has infinite Vapnik-Chervonenkis-dimension (VC-dimension), also called shattering dimension.

Definition 3 (VC-dimension). *Let $\mathcal{X} = \{x_1, \dots, x_n\}$ be a set of n data points labeled with binary labels in $\mathcal{Y} = \{y_1, \dots, y_n\}$. The set of points \mathcal{X} is said to be shattered by a function class \mathcal{F} if for all $y \in \mathcal{Y}^n$ there exists a function $f \in \mathcal{F}$ s.t. $f(x_i) = y_i, i = 1, \dots, n$. The VC-dimension of a function class \mathcal{F} is the size of the largest set of points that can be shattered by \mathcal{F} .*

This result states that there exists at least one data set of infinite size that can be shattered by the function class $f(x) = \text{sign}(\sin(x\omega))$, and a typical example of such a set is $\{2^{-m} : m \in \mathbb{N}\}$ [41]. It does not tell us, however, if an arbitrary set of distinct points with labels in ± 1 can be shattered by this function class. In fact, it is known that this is not the case, and one can easily show that the simple set of evenly spaced points $\{x, 2x, 3x, 4x\}$ with $x \in \mathbb{R}$ can not be shattered by $f(x)$ [41]. To understand whether we can use the sine function to produce the labeling of edge weights of our choice, we can turn to another result, namely that for any rationally independent set of $\{x_1, \dots, x_n\}$ with labels $y_i \in (-1, 1)$, the sine function can approximate these points to arbitrary precision ϵ as shown in [42], i.e.,

$$|\sin(\omega x_i) - y_i| < \epsilon \text{ for } i = 1, \dots, n. \quad (18)$$

In general, the edge weights of graphs that represent TSP instances are not rationally independent.¹ However, in principle they can easily be made rationally independent by adding a finite perturbation ϵ'_i to each edge weight. The results in [42] imply that almost any set of points x_1, \dots, x_n with $0 < x_i < 1$ is rationally independent, so we can choose ϵ'_i to be drawn uniformly at random from $(0, \epsilon_{\max}]$. As long as these perturbations are applied to the edge weights in a way that does not change the optimal tour, as could be done by ensuring that ϵ_{\max} is small enough so that the proportions between edge weights are preserved, we can use this perturbed version of the graph to infer the optimal tour. (Such an ϵ_{\max} can be computed efficiently.) In this way we can guarantee that the ansatz

at depth one can produce arbitrary labelings of our edges, which in turn let us produce expectation values such that only the ones that correspond to edges in the tour of our choice will have positive values. We note that in the analysis we assume real-valued (irrational) perturbations, which of course cannot be represented in the computer. However, by using the results of [42] and approximating ± 1 within a small epsilon, we can get a robust statement where finite precision suffices. For completeness, we provide a proof for this case in section IV C. We, however do not go deeper into this discussion since in fact we do not want to rely on this proof of optimality as a guiding explanation of how the algorithm works.

The reason for this is that in some way, this proof of optimality works *despite* the presence of the TSP graph and not because of it. This is similar in vein to universality results for QAOA-type circuits, where it can be shown that for very specific types of Hamiltonians, alternating applications of the cost and mixer Hamiltonian leads to quantum computationally universal dynamics, i.e. it can reach all unitaries to arbitrary precision [43, 44], but these Hamiltonians are not related to any of the combinatorial optimization problems that were studied in the context of the QAOA. While these results provide valuable insight into the expressivity of the models, in our case they do not inform us about the possibility of a quantum advantage on the learning problem that we study in this work. In particular, we do not know from these results whether the EQC utilizes the information provided by the graph features in a way in which the algorithm benefits from the quantumness of the model, at depth one or otherwise. As it is known that the QAOA applied to ground state finding benefits from interference effects, investigating whether similar results hold for our algorithm is an interesting question that we leave for future work.

Additionally, we note that high expressivity alone does not necessarily lead to a good model, and may even lead to issues in training as the well-studied phenomenon of barren plateaus [15], or a susceptibility to overfitting on the training data. In practice, the best models are those that strike a balance between being expressive enough, and also restricting the search space of the model in a way that suits the given training data. Studying and designing models that have this balance is exactly the goal of geometric learning, and the equivariance we have proven for our model is a helpful geometric prior for learning tasks on graph inputs.

V. NUMERICAL RESULTS

A. Comparison of the EQC and non-equivariant ansatzes on the TSP

After proving that our model is equivariant under node permutations and analytically studying the expressivity of our ansatz, we now numerically study the training and validation performance of this model

¹ The real numbers x_1, \dots, x_n are said to be rationally independent if no integers k_1, \dots, k_n exist such that $x_1 k_1 + \dots + x_n k_n = 0$, besides the trivial solution $k_i = 0 \forall k$. Rational independence also implies the points are not rational numbers, so they are also not numbers normally represented by a computer.

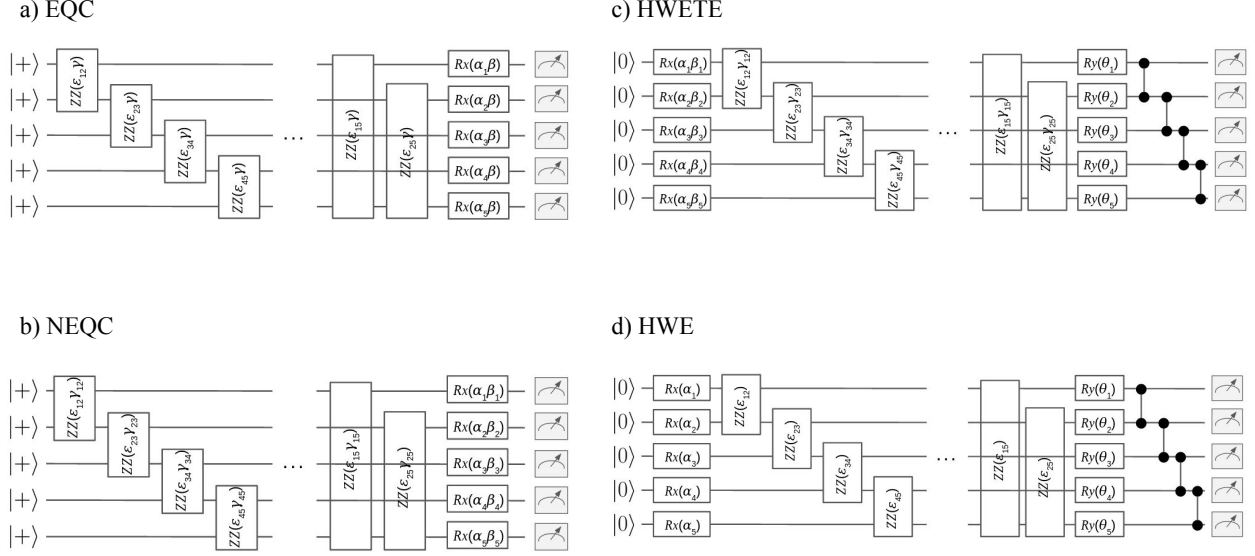


FIG. 4: One layer of each of the circuits studied in this work. a) The EQC with two trainable parameters β, γ per layer. b) The same set of gates as in the EQC, but we break equivariance by introducing one individual free parameter per gate (denoted NEQC). c) Similar to the NEQC, but we start from the all-zero state and add a final layer of trainable one-qubit gates and a ladder of CZ-gates (denoted hardware-efficient with trainable encoding, HWETE). d) Same as the HWETE, but only the single-qubit Y-rotation parameters are trained (denoted HWE).

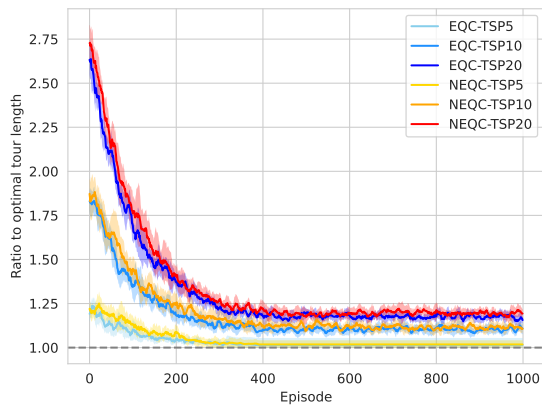
on TSP instances of varying size in a NCO context. The training data set that we use is taken from [3], where the authors propose a novel classical attention approach and evaluate it on a number of geometric learning tasks.² To compute optimal solutions for the TSP instances with 10 and 20 cities we used the library Python-TSP [45].

We evaluate the performance of the EQC on TSP instances with 5, 10 and 20 cities (corresponding to 5, 10, and 20 qubits, respectively). As described in section IV A, the environment is considered as solved by an agent when the running average of the approximation ratio over the past 100 episodes is less than 1.05. Otherwise, each agent will run until it reaches the maximum number of episodes, that we set to be 5000 for all agents. Note that this is merely a convenience to shorten the overall training times, as we have access to the optimal solutions of our training instances. In a realistic scenario where one does not have access to optimal solutions, the algorithm would simply run for a fixed number of episodes or until another convergence criterion is met. When evaluating the final average approximation ratios, we always use the parameter setting that was stored in the final episode, regardless of the final training error. When

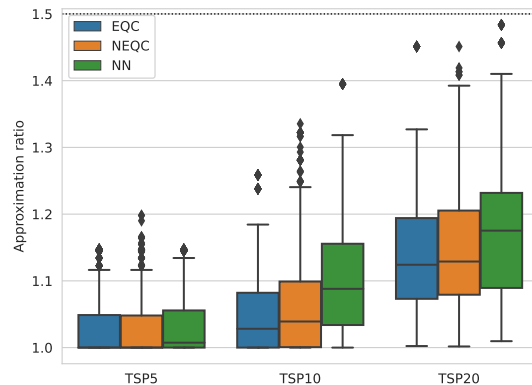
variations in training lead to a slightly worse performance than what was achieved before, we still use the final parameter setting. We do this because as noted above, in a realistic scenario one does not have knowledge about the ratio to the optimal solutions during training. Unless otherwise stated, all models are trained on 100 training instances and evaluated on 100 validation instances.

As we are interested in the performance benefits that we gain by using an ansatz that respects an important graph symmetry, we compare our model to versions of the same ansatz where we gradually break the equivariance property. We start with the simplest case, where the circuit structure is still the same as for the EQC, but instead of having one β_l, γ_l in each layer, every X- and ZZ-gate is individually parametrized. As these parameters are now tied directly to certain one- and two-qubits gates, e.g. an edge between qubits one and two, they will not change location upon a graph permutation and therefore break equivariance. We call this the non-equivariant quantum circuit (NEQC). To go one step further, we take the NEQC and add a variational part to each layer that is completely unrelated to the graph structure: namely a hardware-efficient layer that consists of parametrized Y-rotations and a ladder of CZ-gates. In this ansatz, we have a division between a *data encoding* part and a *variational* part, as is often done in QML. To be closer to standard types of ansatzes often used in QML, we also omit the initial layer of H-gates here and start from the all-zero state (which requires us

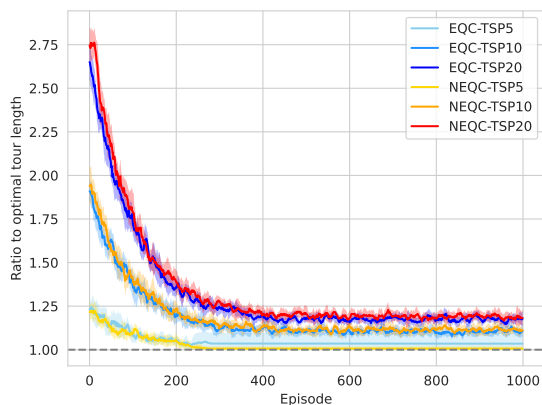
² We note that we have re-computed the optimal tours for all instances that we use, as the data set uploaded by the authors of [3] erroneously contains sub-optimal solutions. This was confirmed with the authors, but at the time of writing of this work their repository has not been updated with the correct solutions.



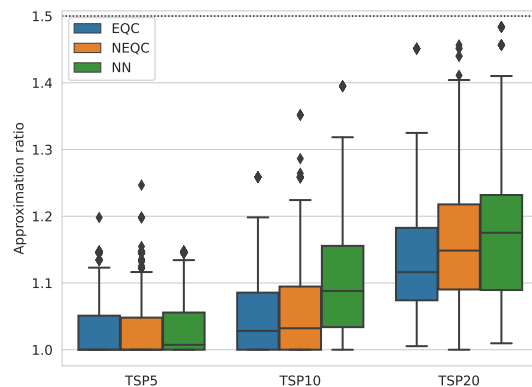
(a) Training performance, 1 layer



(b) Validation performance, 1 layer



(c) Training performance, 4 layers



(d) Validation performance, 4 layers

FIG. 5: Comparison between the EQC and its non-equivariant version (NEQC) where each gate is parametrized separately as described in section V. Results are shown on TSP instances with 5, 10 and 20 cities (TSP5, TSP10 and TSP20, respectively), averaged over ten agents each. To provide a classical baseline, we also show results for the nearest-neighbor heuristic (NN). a) and b) show the training and validation performance for both ansatzes with one layer, while c) and d) show the same for four layers. The dashed, grey line on the left-hand side figures denotes optimal performance. The dotted, black line on the right-hand side figures denotes the upper bound of the Christofides algorithm, a popular classical approximation algorithm that is guaranteed to find a solution that is at most 1.5 times as long as the optimal tour. Figures a) and c) show the running average over the last ten episodes.

to switch the order of X- and ZZ-gates)³. We denote this the hardware-efficient with trainable embedding (HWETE) ansatz. Finally, we study a third ansatz, where we take the HWETE and now only train the Y-rotation gates, and the graph-embedding part of the circuit only serves as a data encoding step. We call this simply the hardware-efficient (HWE) ansatz. A depiction of all ansatzes can be seen in fig. 4.

We start by comparing the EQC to the NEQC on TSP instances with 5, 10 and 20 cities. We show the training and validation results in fig. 5. To evaluate the performance of the models that we study, we com-

pute the ratio to the optimal tour length as shown in eq. (11), as the instances that we can simulate the circuits for are small enough to allow computing optimal tours for.⁴ To provide an additional classical baseline, we also show results for the nearest-neighbor heuristic. This heuristic starts at a random node and selects the closest neighboring node in each step to generate the final tour. The nearest-neighbor algorithm finds a solution quickly also for instances with increasing size, but there is no guarantee that this tour is close to the optimal one. However, as we know the optimal tours

³ However, in practice it did not make a difference whether we started from the all-zero or uniform superposition state in the learning task that we study.

⁴ For reference, the authors of [3], who generated the training instances that we use, stop comparing to optimal solutions at $n = 20$ as it becomes extremely costly to find optimal tours from thereon out.

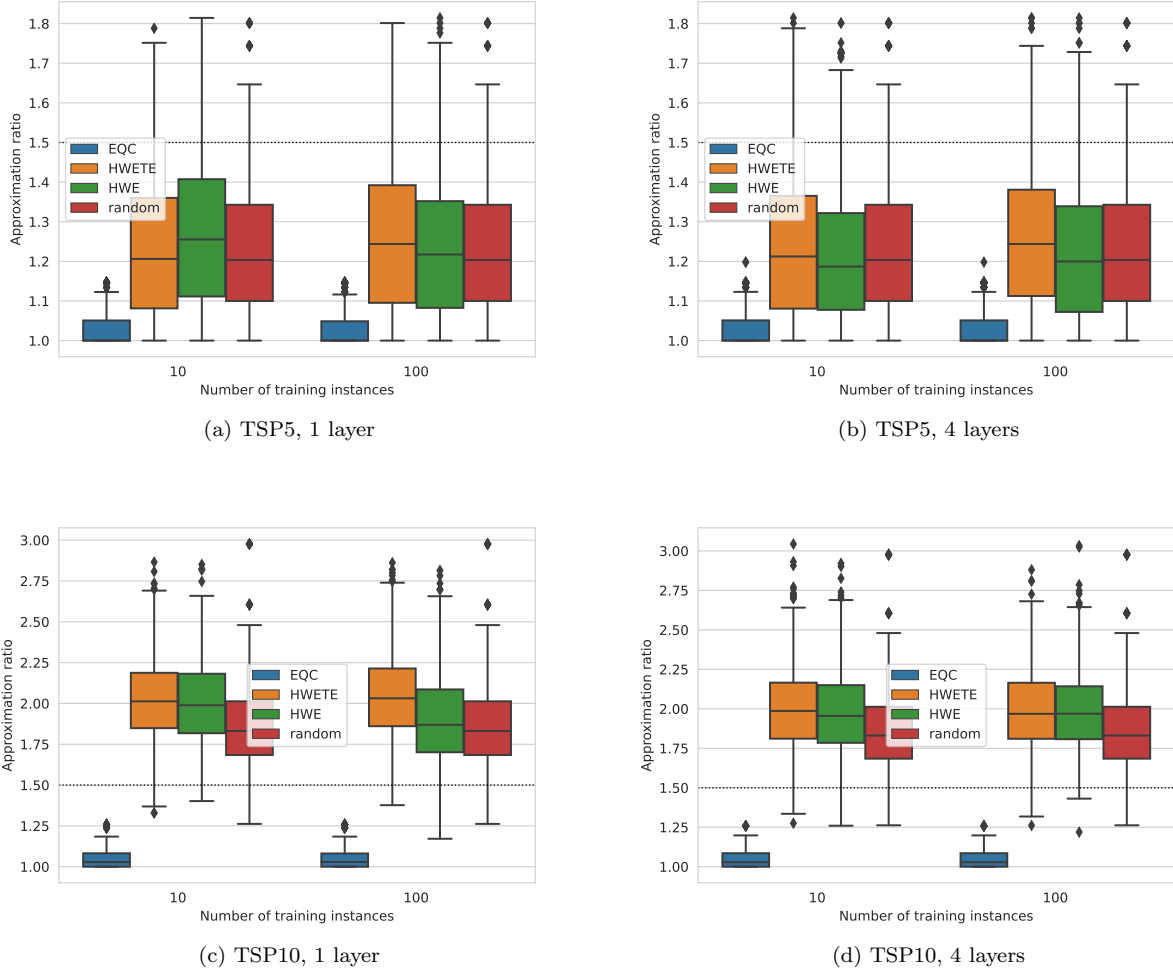


FIG. 6: Comparison between EQC and two hardware-efficient ansatzes where we gradually break the equivariance of the original ansatz. We show results for TSP instances with five and ten cities (TSP5, TSP10 respectively) for models trained on 10 and 100 instances, and with one and four layers. Each box is computed over results for ten agents. The hardware-efficient ansatz with trainable embedding (HWETE) consists of trainable graph encoding layers as those in the EQC, with an additional variational part in each layer that consists of parametrized single-qubit Y-gates and a ladder of CZ-gates. The HWE ansatz is the same as the HWETE, but where the graph-embedding part is not trainable and only the Y-gates in each layer are trained. We also show approximation ratios of a random algorithm, where a random tour is picked as the solution to each instance. The dotted, black lines denote the upper bound of the Christofides algorithm. We see that the HWE ansatzes perform extremely badly and barely outperform picking random tours only in some cases.

for all instances, the nearest-neighbor heuristic provides an easy to understand classical baseline that we can use. Additionally, we add the upper bound given by one of the most widely used approximation algorithms for the TSP (as implemented e.g. in Google OR-Tools): the Christofides algorithm. This algorithm is guaranteed to find a tour that is at most 1.5 times as long as the optimal tour [46]. In the case where any of our models produces validation results that are on average above this upper bound of the Christofides algorithm, we consider it failed, as it is more efficient to use a polynomial approximation algorithm for these instances. The bound is shown as a dotted black line in fig. 5 and fig. 6.

Geometric learning models are expected to be more data-efficient than their unstructured counterparts, as

they respect certain symmetries in the training data. This means that when a number of symmetric instances are present in the training or validation data, the effective size of these data sets is decreased. This usually translates into models that are more resource-efficient in training, e.g. by requiring fewer parameters or fewer training samples. In our comparison of the EQC and the NEQC, we fix the number of training samples and compare the different models in terms of circuit depth and number of parameters to achieve a certain validation error and expect that the EQC will need fewer layers to achieve the same validation performance as the NEQC. This comparison can be seen in fig. 5. In fig. 5 a) and b), we show the training and validation performance of both ansatzes at depth one. For instances with five cities,

both ansatzes perform almost identically on the validation set, where the NEQC performs worse on a few validation instances. As the instance size increases, the gap between EQC and NEQC becomes bigger. We see that even though the two ansatzes are structurally identical, the specific type of parametrizations we choose and the properties of both ansatzes that result from this make a noticeable difference in performance. While the EQC at depth one has only two parameters per layer regardless of instance size, the NEQC's number of parameters per layer depends on the number of nodes and edges in the graph. Despite having much fewer parameters, the EQC still outperforms the NEQC on instances of all sizes. Increasing the depth of the circuits also does not change this. In fig. 5 c) and d) we see that at a depth of four, the EQC still beats the NEQC. The latter's validation performance even slightly decreases with more layers, which is likely due to the increased complexity of the optimization task, as the number of trainable parameters per layer is $\frac{(n-1)n}{2} + n$, which for the 20-city instances means 840 trainable parameters at depth four (compared to 8 parameters in case of the EQC). This shows that at a fraction of the number of trainable parameters, the EQC is competitive with its non-equivariant counterpart even though the underlying structure of both circuits is identical. Compared to the classical nearest-neighbor heuristic, both ansatzes perform well and beat it at all instance sizes, and both ansatzes are also below the approximation ratio upper bound given by the Christofides algorithm on all validation instances.

Next, we compare the EQC to ansatzes in which we introduce additional variational components that are completely unrelated to the training data structure, as described above. We show results for the HWETE and the HWE ansatz in fig. 6. To our own surprise, we did not manage to get satisfactory results with either of those two ansatzes, especially at larger instances, despite an intensive hyperparameter search. Even the HWETE, which is basically identical to the NEQC with additional trainable parameters in each layer, failed to show any significant performance. To gauge how badly those two ansatzes perform, we also show results for an algorithm that selects a random tour for each validation instance in fig. 6. In this figure, we show results for TSP instances with five and ten cities for both ansatzes with one and four layers, respectively. Additionally, we show how the validation performance changes when the models are trained with either a training data set consisting of 10 or 100 instances, in the hopes of seeing improved performance as the size of the training set increases. We see that in neither configuration, the HWETE or HWE outperform the Christofides upper bound on all validation instances. Additionally, in almost all cases those two ansatzes do not even outperform the random algorithm. This example shows that in a complex learning scenario, where the number of permutations of each input instance grows combinatorially with instance size and the number of states in the RL environment grows exponentially with the number of

instances, a simple hardware-efficient ansatz will fail even when the data encoding part of the PQC is motivated by the problem data structure. While increasing the size of the training set and/or the number of layers in the circuit seems to provide small advantages in some cases, it also leads to a decrease in performance in others. On the other hand, the EQC is mostly agnostic to changes in the number of layers or the training data size. Overall, we see that the closer the ansatz is to an equivariant configuration, the better it performs, and picking ansatzes that respect symmetries inherent to the problem at hand is the key to success in this graph-based learning task.

B. Solving the TSP with the QAOA

In section V A, we compared the performance of the EQC to a number of non-equivariant ansatzes and the classical nearest-neighbor heuristic. We have also seen in section III that our ansatz is closely related to that of the QAOA. As the QAOA is arguably the most explored variational quantum optimization algorithm at the time of writing, and due to the structural similarity between the EQC and the QAOA's ansatz, we also compare these two approaches on TSP instances with five cities.

QAOA is implemented as a PQC by a Trotterization of Adiabatic Quantum Computation (AQC) [9]. In general, for AQC, we consider a starting Hamiltonian H_0 , for which both the formulation and the ground state are well known, and a final Hamiltonian H_P , that encodes the combinatorial optimization problem to be solved. The system is prepared in the ground state of the Hamiltonian H_0 and then it is evolved according to the time-dependent Hamiltonian:

$$H(t) := (1 - s(t))H_0 + s(t)H_P,$$

where $s(t)$ is a real function called annealing schedule that satisfies the boundary conditions: $s(0) = 0$ and $s(T) = 1$, with T the duration of the evolution. To implement this as a quantum circuit we use the following approximation:

$$e^{A+B} \approx \left(e^{\frac{A}{r}} e^{\frac{B}{r}} \right)^r, r \rightarrow +\infty, \quad (19)$$

which is known as the Trotter-Suzuki formula. By using this formula to approximate the evolution according to $H(t)$ and by parameterizing time we obtain:

$$e^{-i\beta_p H_0} e^{-i\gamma_p H_P} \dots e^{-i\beta_1 H_0} e^{-i\gamma_1 H_P}. \quad (20)$$

All of these matrices are unitary since the Hamiltonians in the argument of the exponential are all Hermitian. We define a parameter p (integer known as the depth, or level) of QAOA which has the same role as r in eq. (19). Increasing the depth p adds additional layers to the QAOA circuit, and thus more closely approximates the $H(t)$ [9].

In QAOA, all qubits are initialized to $|+\rangle^{\otimes n}$, which is the ground state of $H_0 = \sum_i \sigma_x^{(i)}$. Alternating layers of H_P and H_0 are added to the circuit (p times),

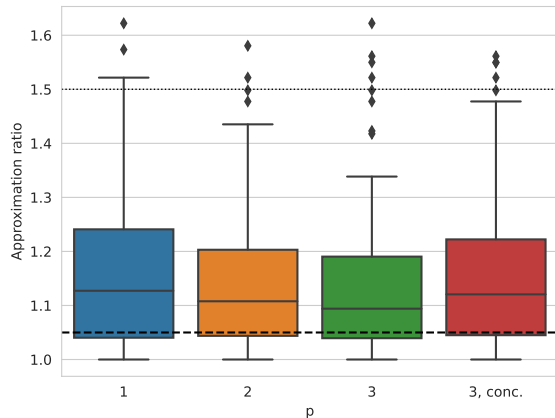


FIG. 7: Approximation ratio of QAOA up to depth three. Dashed black line denotes average final performance of the EQC at depth one during the last 100 iterations of training on the same instances. Last box shows the results for the best parameters found for one instance at $p = 3$ applied to all training instances, following a parameter concentration argument. The dotted, black line denotes the upper bound of the Christofides algorithm.

parameterized by γ and β as defined in eq. (20). The values of γ and β are found by minimizing the expectation value of H_p , and thus approximate the optimal solution to the original combinatorial optimization problem. When using QAOA, we do not solve the TSP directly, but a QUBO representation of this problem. This representation is well-known, and can be found in [47]:

$$\sum_{(i,j) \in \mathcal{E}} \sum_{t=1}^N \frac{\varepsilon_{i,j}}{W} x_{i,t} x_{j,t+1} + \sum_{i \in \mathcal{V}} \left(1 - \sum_{t=1}^N x_{i,t} \right)^2 + \sum_{t=1}^N \left(1 - \sum_{i \in \mathcal{V}} x_{i,t} \right)^2 + \sum_{(i,j) \notin \mathcal{E}} \sum_{t=1}^N x_{i,t} x_{j,t+1}.$$

Here, $\varepsilon_{i,j}$ are the distances between two nodes $i, j \in \mathcal{V}$ and $W := \max_{(i,j) \in \mathcal{E}} \varepsilon_{i,j}$. The variables $x_{v,t}$ are binary decision variables denoting whether node v is visited at step t . We optimize the β and γ parameters for $p = 1$ by performing a uniform random search over the space $[0, 2\pi]^2$, and selecting the best configuration found.

For $p = 2$ and 3 , we optimized the circuit parameters using Constrained Optimization BY Linear Approximation (COBYLA). In addition, similar to [48], we employed a p -dependent initialization technique for the circuit parameters. Specifically, $(p + 1)$ -depth QAOA circuit parameters were initialized with the optimal parameters from the p -depth circuit, as follows:

$$\begin{aligned} \gamma &= (\gamma_1, \dots, \gamma_{p'}, 0), \\ \beta &= (\beta_1, \dots, \beta_{p'}, 0). \end{aligned}$$

This way we are allowing the parameter training procedure to start in a known acceptable state based

on the results of the previous step. In fig. 7 we show our results for five-city instances of the TSP. The approximation ratio shown is derived by dividing the tour length of the best feasible solution, measured as the output of the trained QAOA circuit, by the optimal tour length of the respective instance. In addition, we compute results for two different $p = 3$ QAOA circuits: the first is trained in the procedure described above (where the parameters are trained for each instance). The second uses the parameters of the best QAOA circuit out of those for all instances evaluated at $p = 3$, following a concentration of parameters argument as presented in [49]. The second method is closer to what is done in a ML context, where one set of parameters is used to evaluate the performance on all validation samples.

Due to the number of qubits required to formulate a QUBO for the TSP, we were not able to run QAOA for all TSP instances. For example, an instance with six cities already requires 25 qubits⁵. A different formulation of the QUBO problem presented in [50], that needs $O(n \log(n))$ qubits, avoids this issue by modifying the circuit design. However, this proposal increases the circuit depth considerably and is therefore ill-suited for the NISQ era.

In fig. 7, we can see that finding a good set of parameters for QAOA to solve TSP is hard even for five-city instances. We note that the performance of QAOA improves with higher p , however, QAOA performance is still far from matching the approximation ratios obtained by EQC even for $p = 3$, which can be seen in fig. 7 as a black dashed line. Furthermore, we note that significant computational effort is required to obtain these results: methods like COBYLA are based on gradient descent, which requires us to evaluate the circuit many times until either convergence or the maximum number of iterations is reached. We also note that due to the heuristic optimization of the QAOA parameters themselves, we are not guaranteed that the configuration of parameters is optimal, which may result in either insufficient iterations to converge or premature convergence to sub-optimal parameter values. In an attempt to mitigate this, we tested several optimizers (Adam, SPSA, BFGS and COBYLA) and used the best results, which were those found by COBYLA.

We see that already on these small instances, the QAOA requires significantly deep circuits to achieve good results, that may be out of reach in a NISQ setting. The EQC on the other hand i) uses a number of qubits that scales linearly with the number of nodes of the input graph, and ii) already shows good performance at depth one for instances with up to 20 cities.

⁵ We can fix the choice of the first city to be visited without loss of generality, requiring only $(n - 1)^2$ variables to formulate the QUBO.

VI. DISCUSSION

After providing analytic insight on the expressivity of our ansatz, we have numerically investigated the performance of our EQC model on TSP instances with 5, 10, and 20 cities (corresponding to 5, 10, 20 qubits respectively), and compared them to other types of ansatzes that do not respect any graph symmetries. To get a fair comparison, we designed PQC models that gradually break the equivariance property of the EQC and assessed their performance. We find that ansatzes that contain structures that are completely unrelated to the input data structure are extremely hard to train for this learning task where the size of the state space scales exponentially in the number of input nodes of the graph. Despite much effort and hyperparameter optimization, we did not manage to get satisfactory results with these ansatzes. The EQC on the other hand works almost out-of-the-box, and achieves good generalization performance with minimal hyperparameter tuning and relatively few trainable parameters. We have also compared using the EQC in a neural combinatorial optimization scheme with the QAOA, and find that even on TSP instances with only five cities the NCO approach significantly outperforms the QAOA. In addition to training the QAOA parameters for every instance individually, we have also investigated the performance in light of known parameter concentration results that state that in some cases, parameters found on one instance perform well on average for other instances of the same problem. While this is true in the case of the TSP instances we investigate here as well, the overall performance is still worse than that of the EQC.

Comparing our algorithm to the QAOA is also interesting from a different perspective. In section III we have seen that our ansatz can be regarded as a special case of a QAOA-type ansatz, where instead of encoding a problem Hamiltonian we encode a graph instance directly, and include mixing terms only for a problem-dependent subset of qubits. This lets us derive an exact formulation of the expectation values of our model at depth one from those of the QAOA given in [40]. For the QAOA, it is known that in the limit of infinite depth, it can find the ground state of the problem Hamiltonian and therefore the optimal solution to a given combinatorial optimization problem [9]. Additionally, it has been shown that even at low depth, the probability distributions generated by QAOA-type circuits are hard to sample from classically [51]. These results give a clear motivation of why using a quantum model in these settings can provide a potential advantage. While our model is structurally almost identical to that of the QAOA, in our case the potential for advantage is less clear. We saw in eq. (17) that at depth one, in each step the expectation value of each edge that we consider to be selected consists of i) a term corresponding to the edge between the last added node and the candidate node, and ii) all outgoing edges from the candidate node. So our model considers the one-step neighborhood of each candidate node at depth one. In the case of the

TSP it is not clear whether this can provide a quantum advantage for the learning task as specified in section IV A. In terms of QAOA, it was shown that in order to find optimal solutions, the algorithm has to “see the whole graph” [52], meaning that all edges in the graph contribute to the expectation values used to minimize the energy. To alleviate this strong requirement on depth, a recursive version of the QAOA (RQAOA) was introduced in [53]. It works by iteratively merging edges in the problem graph based on their correlation, and thereby gradually reducing the problem to a smaller instance that can be solved efficiently by a classical algorithm, e.g. by brute-force search. The authors of [53] show that the depth-one RQAOA outperforms QAOA with constant depth p , and that RQAOA achieves an approximation ratio of one for a family of Ising Hamiltonians. While the RQAOA at depth one can be considered a classical algorithm due to its efficient simulability, a subsequent work compared higher depth versions of RQAOA to the best known generic classical algorithm for graph coloring and showed that these deeper versions of RQAOA outperform the classical approach [54]. This suggests that there is a potential for advantage in this setting as well. The node selection process performed by our algorithm with the EQC used as the ansatz is similar to RQAOA, where instead of merging edges, the mixer terms for nodes that have already been selected are turned off, therefore effectively turning expectation values of edges corresponding to unavailable nodes to zero. It is an interesting question whether this type of model can lead to a quantum advantage on the TSP problem that we study here, and we leave this for future work.

VII. CONCLUSIONS

Inspired by classical geometric deep learning and in an effort to illustrate the importance of problem-tailored ansatzes for QML, we have proposed an ansatz for learning on weighted graphs in this work. This ansatz respects an important graph symmetry, namely equivariance under node permutations. By designing our PQC such that it inherently respects this symmetry, we have encoded a problem-motivated bias into our model. A model that does not inherently respect this symmetry will treat each permutation of a training instance as a separate data point and thus has to learn good parameter settings for each individual permutation. Our equivariant model on the other hand, “recognizes” a permutation of a graph instance and will therefore not need separate training data points to learn parameters for each possible permutation, of which there are combinatorially many. Classically, it was proven that these types of models require fewer training data to generalize well than their unstructured counterparts [55]. It is an interesting question for future work whether these types of statements can also be made about quantum models. Our results illustrate the need for QML ansatzes that are motivated by the training data structure.

We introduced such an ansatz for learning tasks on weighted graphs, however, more research is required to find suitable ansatzes for other types of data as well in order to make a near-term advantage in QML possible in the future.

Acknowledgements

AS thanks Elies Gil-Fuster and Radoica Draskic for valuable discussions about geometric deep learning.

AS, MC and SY are funded by the German Ministry for Education and Research (BMB+F) in the project QAI2-Q-KIS under grant 13N15587. VD is supported by the Dutch Research Council (NWO/OCW), as part of the Quantum Software Consortium programme (project number 024.003.037). VD also acknowledges the support by the project NEASQC funded from the European Union's Horizon 2020 research and innovation programme (grant agreement No 951821).

-
- [1] Quentin Cappart, Didier Chételat, Elias Khalil, Andrea Lodi, Christopher Morris, and Petar Veličković. Combinatorial optimization and reasoning with graph neural networks. *arXiv preprint arXiv:2102.09544*, 2021.
 - [2] Yoshua Bengio, Andrea Lodi, and Antoine Prouvost. Machine learning for combinatorial optimization: a methodological tour d'horizon. *European Journal of Operational Research*, 290(2):405–421, 2021.
 - [3] Oriol Vinyals, Meire Fortunato, and Navdeep Jaitly. Pointer networks. *arXiv preprint arXiv:1506.03134*, 2015.
 - [4] Hanjun Dai, Elias B Khalil, Yuyu Zhang, Bistra Dilkina, and Le Song. Learning combinatorial optimization algorithms over graphs. *arXiv preprint arXiv:1704.01665*, 2017.
 - [5] Azalia Mirhoseini, Anna Goldie, Mustafa Yazgan, Joe Jiang, Ebrahim Songhori, Shen Wang, Young-Joon Lee, Eric Johnson, Omkar Pathak, Sungmin Bae, et al. Chip placement with deep reinforcement learning. *arXiv preprint arXiv:2004.10746*, 2020.
 - [6] Mohammadreza Nazari, Afshin Oroojlooy, Lawrence V Snyder, and Martin Takáč. Reinforcement learning for solving the vehicle routing problem. *arXiv preprint arXiv:1802.04240*, 2018.
 - [7] Michael M Bronstein, Joan Bruna, Taco Cohen, and Petar Veličković. Geometric deep learning: Grids, groups, graphs, geodesics, and gauges. *arXiv preprint arXiv:2104.13478*, 2021.
 - [8] Marco Cerezo, Andrew Arrasmith, Ryan Babbush, Simon C Benjamin, Suguru Endo, Keisuke Fujii, Jarrod R McClean, Kosuke Mitarai, Xiao Yuan, Lukasz Cincio, et al. Variational quantum algorithms. *Nature Reviews Physics*, 3(9):625–644, 2021.
 - [9] Edward Farhi, Jeffrey Goldstone, and Sam Gutmann. A quantum approximate optimization algorithm. *arXiv preprint arXiv:1411.4028*, 2014.
 - [10] Tavis Bennett, Edric Matwiejew, Sam Marsh, and Jingbo B Wang. Quantum walk-based vehicle routing optimisation. *Frontiers in Physics*, page 692, 2021.
 - [11] Harper R Grimsley, Sophia E Economou, Edwin Barnes, and Nicholas J Mayhall. Adapt-vqe: An exact variational algorithm for fermionic simulations on a quantum computer. *arXiv preprint arXiv:1812.11173*, 2018.
 - [12] Alberto Peruzzo, Jarrod McClean, Peter Shadbolt, Man-Hong Yung, Xiao-Qi Zhou, Peter J Love, Alán Aspuru-Guzik, and Jeremy L O'brien. A variational eigenvalue solver on a photonic quantum processor. *Nature communications*, 5(1):1–7, 2014.
 - [13] Abhinav Kandala, Antonio Mezzacapo, Kristan Temme, Maika Takita, Markus Brink, Jerry M Chow, and Jay M Gambetta. Hardware-efficient variational quantum eigensolver for small molecules and quantum magnets. *Nature*, 549(7671):242–246, 2017.
 - [14] Marcello Benedetti, Erika Lloyd, Stefan Sack, and Mattia Fiorentini. Parameterized quantum circuits as machine learning models. *Quantum Science and Technology*, 4(4):043001, 2019.
 - [15] Jarrod R McClean, Sergio Boixo, Vadim N Smelyanskiy, Ryan Babbush, and Hartmut Neven. Barren plateaus in quantum neural network training landscapes. *Nature communications*, 9(1):1–6, 2018.
 - [16] Andrew Arrasmith, M Cerezo, Piotr Czarnik, Lukasz Cincio, and Patrick J Coles. Effect of barren plateaus on gradient-free optimization. *Quantum*, 5:558, 2021.
 - [17] Carlos Ortiz Marrero, Mária Kieferová, and Nathan Wiebe. Entanglement-induced barren plateaus. *PRX Quantum*, 2(4):040316, 2021.
 - [18] Patrick van der Smagt and Gerd Hirzinger. Why feed-forward networks are in a bad shape. In *International Conference on Artificial Neural Networks*, pages 159–164. Springer, 1998.
 - [19] Code used in this work https://github.com/askolik/eqc_for_nco.
 - [20] John Jumper, Richard Evans, Alexander Pritzel, Tim Green, Michael Figurnov, Olaf Ronneberger, Kathryn Tunyasuvunakool, Russ Bates, Augustin Židek, Anna Potapenko, et al. Highly accurate protein structure prediction with alphafold. *Nature*, 596(7873):583–589, 2021.
 - [21] Kathryn Tunyasuvunakool, Jonas Adler, Zachary Wu, Tim Green, Michal Zielinski, Augustin Židek, Alex Bridgland, Andrew Cowie, Clemens Meyer, Agata Laydon, et al. Highly accurate protein structure prediction for the human proteome. *Nature*, 596(7873):590–596, 2021.
 - [22] Yann LeCun, Yoshua Bengio, et al. Convolutional networks for images, speech, and time series. *The handbook of brain theory and neural networks*, 3361(10):1995, 1995.
 - [23] Robin M Schmidt. Recurrent neural networks (rnns): A gentle introduction and overview. *arXiv preprint arXiv:1912.05911*, 2019.
 - [24] Zonghan Wu, Shirui Pan, Fengwen Chen, Guodong Long, Chengqi Zhang, and S Yu Philip. A comprehensive survey on graph neural networks. *IEEE transactions on neural networks and learning systems*, 32(1):4–24, 2020.
 - [25] Jie Zhou, Ganqu Cui, Shengding Hu, Zhengyan Zhang, Cheng Yang, Zhiyuan Liu, Lifeng Wang, Changcheng Li, and Maosong Sun. Graph neural net-

- works: A review of methods and applications. *AI Open*, 1:57–81, 2020.
- [26] Elman Mansimov, Omar Mahmood, Seokho Kang, and Kyunghyun Cho. Molecular geometry prediction using a deep generative graph neural network. *Scientific reports*, 9(1):1–13, 2019.
- [27] Jianwu Long et al. A graph neural network for superpixel image classification. In *Journal of Physics: Conference Series*, volume 1871, page 012071. IOP Publishing, 2021.
- [28] Iris Cong, Soonwon Choi, and Mikhail D Lukin. Quantum convolutional neural networks. *Nature Physics*, 15(12):1273–1278, 2019.
- [29] Guillaume Verdon, Trevor McCourt, Enxhell Luzhnica, Vikash Singh, Stefan Leichenauer, and Jack Hidary. Quantum graph neural networks. *arXiv preprint arXiv:1909.12264*, 2019.
- [30] Louis-Paul Henry, Slimane Thabet, Constantin Dalyac, and Loïc Henriet. Quantum evolution kernel: Machine learning on graphs with programmable arrays of qubits. *Physical Review A*, 104(3):032416, 2021.
- [31] Jin Zheng, Qing Gao, and Yanxuan Lü. Quantum graph convolutional neural networks. In *2021 40th Chinese Control Conference (CCC)*, pages 6335–6340. IEEE, 2021.
- [32] Yanhu Chen, Cen Wang, Hongxiang Guo, et al. Novel architecture of parameterized quantum circuit for graph convolutional network. *arXiv preprint arXiv:2203.03251*, 2022.
- [33] Péter Mernyei, Konstantinos Meichanetzidis, and İsmail İlkan Ceylan. Equivariant quantum graph circuits. *arXiv preprint arXiv:2112.05261*, 2021.
- [34] Martín Larocca, Frédéric Sauvage, Faris M. Sbahi, Guillaume Verdon, Patrick J. Coles, and M. Cerezo. Group-invariant quantum machine learning. *arXiv preprint arXiv:2205.02261*, 2022.
- [35] Richard S Sutton and Andrew G Barto. *Reinforcement learning: An introduction*. MIT press, 2018.
- [36] Volodymyr Mnih, Koray Kavukcuoglu, David Silver, Andrei A Rusu, Joel Veness, Marc G Bellemare, Alex Graves, Martin Riedmiller, Andreas K Fiedelnd, Georg Ostrovski, et al. Human-level control through deep reinforcement learning. *nature*, 518(7540):529–533, 2015.
- [37] Samuel Yen-Chi Chen, Chao-Han Huck Yang, Jun Qi, Pin-Yu Chen, Xiaoli Ma, and Hsi-Sheng Goan. Variational quantum circuits for deep reinforcement learning. *IEEE Access*, 8:141007–141024, 2020.
- [38] Owen Lockwood and Mei Si. Reinforcement learning with quantum variational circuit. In *Proceedings of the AAAI Conference on Artificial Intelligence and Interactive Digital Entertainment*, volume 16, pages 245–251, 2020.
- [39] Andrea Skolik, Sofiene Jerbi, and Vedran Dunjko. Quantum agents in the gym: a variational quantum algorithm for deep q-learning. *arXiv preprint arXiv:2103.15084*, 2021.
- [40] Asier Ozaeta, Wim van Dam, and Peter L McMahon. Expectation values from the single-layer quantum approximate optimization algorithm on ising problems. *arXiv preprint arXiv:2012.03421*, 2020.
- [41] Mehryar Mohri. Foundations of machine learning. <https://cs.nyu.edu/~mohri/ml16/sol2.pdf>, 2016.
- [42] Gilbert H Harman, Sanjeev R Kulkarni, and Hariharan Narayanan. $\sin(\omega x)$ can approximate almost every finite set of samples. *Constructive Approximation*, 42(2):303–311, 2015.
- [43] Seth Lloyd. Quantum approximate optimization is computationally universal. *arXiv preprint arXiv:1812.11075*, 2018.
- [44] Mauro ES Morales, Jacob D Biamonte, and Zoltán Zimborás. On the universality of the quantum approximate optimization algorithm. *Quantum Information Processing*, 19(9):1–26, 2020.
- [45] Python-tsp <https://github.com/fillipe-gsm/python-tsp>.
- [46] Nicos Christofides. Worst-case analysis of a new heuristic for the travelling salesman problem. Technical report, Carnegie-Mellon Univ Pittsburgh Pa Management Sciences Research Group, 1976.
- [47] Andrew Lucas. Ising formulations of many np problems. *Frontiers in physics*, 2:5, 2014.
- [48] Leo Zhou, Sheng-Tao Wang, Soonwon Choi, Hannes Pichler, and Mikhail D Lukin. Quantum approximate optimization algorithm: Performance, mechanism, and implementation on near-term devices. *Physical Review X*, 11(2):021067, 2020.
- [49] Fernando G. Brandao, Michael Broughton, Edward Farhi, Sam Gutmann, and Hartmut Neven. For fixed control parameters the quantum approximate optimization algorithm’s objective function value concentrates for typical instances. *arXiv preprint arXiv:1812.04170*, 2018.
- [50] Adam Glos, Alexandra Krawiec, and Zoltán Zimborás. Space-efficient binary optimization for variational computing. *arXiv preprint arXiv:2009.07309*, 2020.
- [51] Edward Farhi and Aram W Harrow. Quantum supremacy through the quantum approximate optimization algorithm. *arXiv preprint arXiv:1602.07674*, 2016.
- [52] Edward Farhi, David Gamarnik, and Sam Gutmann. The quantum approximate optimization algorithm needs to see the whole graph: A typical case. *arXiv preprint arXiv:2004.09002*, 2020.
- [53] Sergey Bravyi, Alexander Kliesch, Robert Koenig, and Eugene Tang. Obstacles to variational quantum optimization from symmetry protection. *Physical review letters*, 125(26):260505, 2020.
- [54] Sergey Bravyi, Alexander Kliesch, Robert Koenig, and Eugene Tang. Hybrid quantum-classical algorithms for approximate graph coloring. *Quantum*, 6:678, 2022.
- [55] Song Mei, Theodor Misiakiewicz, and Andrea Montanari. Learning with invariances in random features and kernel models. In *Conference on Learning Theory*, pages 3351–3418. PMLR, 2021.

Appendix A: Proof of equivariance of ansatz

Proof of theorem 1. First, we show that one layer of the ansatz is equivariant under permutation of graph vertices. Our ansatz is initialized in the uniform superposition, which is permutation invariant by definition, so we only have to show that the unitaries each layer in the ansatz is equivariant. Each layer consists of two terms: $U_N(\alpha, \beta_j)$ and $U_G(\mathcal{E}, \gamma_j)$. We need to show that both of these fulfill the equivariance property. The first term contains only single-qubit operations, where each operation is defined w.r.t. vertices in \mathcal{G} . For an arbitrary quantum state $|\psi\rangle$ defined on a register of n qubits, a permutation of qubits

corresponds to applying a series of SWAP-gates on those qubits. The SWAP operation leaves the individual quantum states unchanged, and merely reassigns them to a new position in the register, therefore fulfilling the above equivariance property. The second term U_G consists of two-qubit ZZ-operators, each weighted by a trainable parameter γ_j and an edge weight ε_{ij} . ZZ-operators are diagonal and therefore commute, so the order in which they are executed does not matter. In addition, the assignment of edge weights to the given $Z_i Z_j$ is determined by the adjacency matrix A of the graph, and therefore a permutation on the adjacency matrix directly translates to a re-assignment of edge weights to their corresponding $Z_i Z_j$ according to the permuted adjacency matrix, which makes the second term equivariant as well. Additionally, the permutation invariance of the trainable parameters is guaranteed by using one shared parameter for each ZZ-term or X-rotation in each layer. Note that parameters not being tied to specific edge weights is necessary, because otherwise trainable parameters would be assigned to different edge weights depending on the specific graph permutation, which would break equivariance.

Now that we have shown that a single layer in our ansatz is equivariant under permutation of vertices, it remains to show that the composition of multiple layers is equivariant as well. This easily follows from the above, as we have already shown that the permutation of the single-qubit operators corresponding to vertices is akin to a SWAP operation on a quantum state $|\psi\rangle$, that itself is permutation equivariant. In particular, this quantum state can be the state given by a previous layer of the ansatz. The equivariance of multiple executions of the two-qubit operations in the ansatz then also follows directly from the above. \square

Note that the above is not true for arbitrary initial states of the circuit, but only for those that satisfy the equivariance property as well. Any non-equivariant part in the ansatz will cause the whole ansatz to be non-equivariant. In the main text, we have briefly discussed scenarios in which each node in the graph corresponds to multiple qubits in the ansatz. The above proof holds for the one qubit case, and whether an ansatz with multiple qubits per node will still be equivariant depends on the chosen mapping of node and edge features. A trivial example where the above holds, is when multiple node features are encoded via single-qubit rotations on each additional qubit, and edge features are still encoded in form of commuting two-qubit gates as above.

Appendix B: Proof that ansatz can generate optimal tours for rationally independent set of edge weights

In this section, we show how the fact that the sine function can approximate an arbitrary set of rationally independent values $\{x_1, \dots, x_n\}$ with labels

$y_i \in [-1, 1]$ can be used to prove that our ansatz at depth one can construct the optimal tour for a graph with edge weights that are rationally independent.

Theorem 4 (Ansatz can generate optimal tours for rationally independent edge weights). *There exists a setting $(\beta, \gamma)^*$ for each graph instance of the symmetric TSP such that the ansatz at depth one described in section III will produce the optimal tour T^* with the node selection process described in definition 2, given that the edge weights ε_{ij} of the graph are rationally independent and $\varepsilon_{ij}\gamma \neq \frac{\pi}{4} + n\pi \forall n \in \mathbb{Z}$.*

Proof. As known from [42], we can find a parameter ω such that we can approximate an arbitrary labeling in $[-1, 1]$ for our rationally independent edge weights with the sine function. Given that this labeling exists, we now show how to use this labeling to generate the optimal tour with the EQC at depth one.

For $p = 1$, we can compute the analytic form of the expectation values of our circuit as defined in eq. (13) and eq. (14) as the following, by a similar derivation as in [40],

$$\langle O_{v_l} \rangle = \varepsilon_{v_{t-1}, v_l} \cdot \sin(\beta\pi) \sin(\varepsilon_{v_{t-1}, v_l} \gamma) \cdot \prod_{\substack{(v_l, k) \in \mathcal{E} \\ k \neq v_{t-1}}} \cos(\varepsilon_{v_l, k} \gamma), \quad (\text{B1})$$

where v_{t-1} is the last node in the partial tour and v_l is the candidate node. By the identity $\cos(\theta) = \sin(\frac{\pi}{2} - \theta)$ we can rewrite eq. (17) as

$$\langle O_{v_l} \rangle = \varepsilon_{v_{t-1}, v_l} \cdot \sin(\beta\pi) \sin(\varepsilon_{v_{t-1}, v_l} \gamma) \cdot \prod_{\substack{(v_l, k) \in \mathcal{E} \\ k \neq v_{t-1}}} \sin\left(\frac{\pi}{2} - \varepsilon_{v_l, k} \gamma\right). \quad (\text{B2})$$

Let us now assume that we want to construct a fixed (but arbitrary) tour T . First, we notice that the term $\sin(\beta\pi)$ does not depend on v_{t-1} or v_l and is the same for all v_l . This means that this term can merely flip the sign of all $\langle O_{v_l} \rangle$, and from now on w.l.o.g. we assume that β is such that the term is positive. Now we can again formulate the tour generation task in terms of a binary classification problem, where we want to find a configuration of labels for our remaining sin terms in eq. (B2) s.t. the product will have the highest expectation value in each node selection step for the edge that produces the ordering we have chosen for T . Again, we can accomplish this for arbitrary settings of edge weights by only considering the sign of the resulting product. This means that we have to find an assignment of the edges ε_{ij} to the classes f_{\pm} that at each step of the node selection process will lead to the node being picked that we specify in T . As all edges can occur in the above products multiple times during the node selection process, this is a non-trivial task. However, if we can guarantee that each $\langle O_{v_l} \rangle_t$ at node selection step t contains at least one *unique term* that is only present in this specific expectation value, we can use this term to control the

sign of this specific value. Each ε_{ij} occurs either in the leading term $\sin(\varepsilon_{ij}\gamma)$ (corresponding to the candidate edge to be potentially added in the next step) or in the product term as $\sin(\frac{\pi}{2} - \varepsilon_{ij}\gamma)$ (corresponding to an outgoing edge from the current candidate). We can easily see that the leading term *only* appears in the case when we ask for this specific ε_{ij} to be the next edge in the tour, and from definition 2 we know that this only happens once in the node selection process. In all other expectations, ε_{ij} appears only with the “offset” of $\frac{\pi}{2}$. This means that this leading term is the unique term that we are looking for, as long as $\sin(\varepsilon_{ij}\gamma) \neq \sin(\frac{\pi}{2} - \varepsilon_{ij}\gamma)$, so as long as $\sin(\varepsilon_{ij}\gamma) \neq \cos(\varepsilon_{ij}\gamma)$. We know that $\cos(\theta) = \sin(\theta)$ for $\theta = \frac{\pi}{4} + n\pi$ with $n \in \mathbb{Z}$. So as long as

$$\varepsilon_{ij}\gamma \neq \frac{\pi}{4} + n\pi \quad \forall n \in \mathbb{Z}, \varepsilon_{ij} \in \mathcal{E}, \quad (\text{B3})$$

and all ε_{ij} are unique, our ansatz can construct the

desired tour T . In this case, we have a guarantee that we can construct the tour T for any configuration of edges that fulfills eq. (B3). In particular, this means that we can construct the optimal tour in this way. \square

Additionally, due to equivariance of our model under node permutations, it is sufficient to find just one of these settings for any tour T and use this to construct the optimal tour. We can do this because once we have found a labeling of the edges for the classes f_{\pm} that produces a given tour sequence, we can simply reshuffle our nodes s.t. this sequence of the “physical nodes” (indices corresponding to qubits) will produce the optimal tour for our “logical nodes” ((x, y) coordinates of graph nodes). However, note that this can not be used to trivially find the optimal tour, as it amounts to trying all $\frac{(n-1)!}{2}$ possible tours.